DOI: 10.1143/JPSJ.81.064503

Rapid Collapse of a Plasma Sawtooth Oscillation in the HT-7 Tokamak

Liqing XU*, Liqun HU, Kaiyun CHEN, Erzhong LI, Jizong ZHANG, Ruijie ZHOU, Ming XU, and Yebin CHEN

Institute of Plasma Physics, Chinese Academy of Science, Hefei 230031, China

(Received January 4, 2012; accepted April 16, 2012; published online May 30, 2012)

The rapid collapse of a sawtooth oscillation which is characterized by the absence of any discernible precursor oscillation in the HT-7 tokamak has been observed in detail on a fast time scale. The contour plot of the raw data of soft-x-ray signals shows that sawtooth crash simultaneously on both the high field side and the low field side with symmetry. Only spatial structure of sawtooth exists in the whole sawtooth period. A larger heat outflow and profile of emission intensities flatten during sawtooth crash by means of soft x-ray tomography. The plausible interpretation is the stochastization of magnetic field lines lead to a transition from semicollisional to collisionless reconnection regimes during non-linear pre-crash phase in which the growth rate is rapidly increased and no any discernible precursor oscillation.

KEYWORDS: fast crash, sawtooth, tokamak

1. Introduction

Since it was first discovered by Von Goeler *et al.*,[1] sawtooth collapse has been observed on every tokamak during normal discharges. The essential characteristics of the sawtooth are the fast crash of the central temperature, density and other parameters. The resistive internal kink mode was invoked by Kadomtsev[2] to explain the crash phase of the oscillations. In this model sawtooth collapse is a magnetic reconnection process, in which a fast change of helical magnetic flux and a large electric field are induced. The Kadomtsev model has been generally believed to explain the sawtooth oscillations in earlier tokamaks but since there is no linear stability threshold for the $m = n = 1$ kink mode in cylindrical geometry if $q_0 < 1$, the quiescent ramp phase of the sawtooth cycle is difficult to explain, and its duration is outside the scope of the model.[3] Followed Kadomtsev model, other models[4–6] have been proposed to explain the sawtooth trigger mechanism, but those different models may be only applicable to specific machines.

Later, rapid collapses of sawtooth oscillations were observed in the JET[7] tokamak and FTU[8,9] tokamak and the usual resistive reconnection rate of the $m = 1$ mode cannot explain the experimentally observed fast crash. In order to explain the fast crash time, many fast reconnection models were proposed. Two-fluid linear magnetohydrodynamic[10] theory or the internal kink mode was studied in finite β regimes. Fast reconnection model was proposed by considering electron inertia,[11,12] parallel electron viscosity[13] and other non-ideal kinetic effects[14] in the thin current layer. Another kind of explanation, which involved the nonlinear evolution of the magnetic islands, is that a magnetic turbulence region formed in the plasma core due to mode interaction,[15] secondary resistive g-modes[16] and nonlinear dynamics,[17] before the $m = 1$ island fills the plasma central region. Nonetheless Fast magnetic reconnection, so far, has been a long-debated problem in tokamak plasma physics, and the trigger mechanism is still an insoluble mystery.

Recently, stochastization of magnetic field lines during the crash maybe a candidate explanation to sawtooth crash in the ASDEX Upgrade tokamak and other tokamaks.[18–22] In ASDEX Upgrade, it was shown that amplitudes of the primary $(1, 1)$ mode together with its harmonics are sufficient to stochastize the region if the central q is less than 0.85–0.9, which allows one to explain the existence of the mode after the sawtooth collapse. Also magnetohydrodynamic oscillations with two frequencies develop before the crash; their frequency ratio is close to the conjugate golden ratio $G = f_2/f_1 = (\sqrt{5} - 1)/2 \approx 0.618$.

Different kinds of sawtooth and $m = 1$ mode activities have been observed in LHCD plasmas on HT-7.[23–28] Even after the sawtooth was completely suppressed, the $m = 1$ mode survived[23] during the LHCD stage, which was also observed on ASDEX.[29] The rapid collapse of a sawtooth oscillation which is characterized by the absence of any discernible precursor oscillation has been observed in detail on a fast time scale on HT-7 Tokamak, which was also observed on DIII-D.[30] More detailed observations will be given in this paper and analytical result shows that rapid collapse of a sawtooth oscillation is consistent with the stochastic field model.

The rest of this paper is organized as follows: the experimental setup and observations are presented in §2 and §3 respectively, followed by a discussion and the summary of the main results in §4 and §5.

2. Experimental Setup

The HT-7 tokamak has major and minor radii of $R = 122\,\text{cm}$ and $a = 27\,\text{cm}$, respectively. The device operates normally at the following parameters: plasma current $I_p \sim 100$–$250\,\text{kA}$ with a duration of 3.5 s. Central chord-averaged electron density $(0.8\text{–}5.0) \times 10^{19}\,\text{m}^{-3}$. Central electron and ion temperatures $T_e(0) = 0.5\text{–}1.0\,\text{keV}$ and $T_i(0) = 0.5\,\text{keV}$. Energy confinement time $\tau_E = 15\,\text{ms}$ and effective charge $Z_{\text{eff}} = 2\text{–}3$, the toroidal beta is about 0.3% and the poloidal beta is about 0.3–0.5. The typical sawtooth crash time in LHCD plasma is about 50–100 μs, while the characteristic reconnection time $\tau_k = 0.5\sqrt{(\tau_R \tau_A)}$ (τ_R is resistive time and τ_A is Alfven time) is about 300–400 μs. The typical sawtooth reversal surface in LHCD plasmas is at about a/3. The large

*E-mail: lqxu@ipp.ac.cn

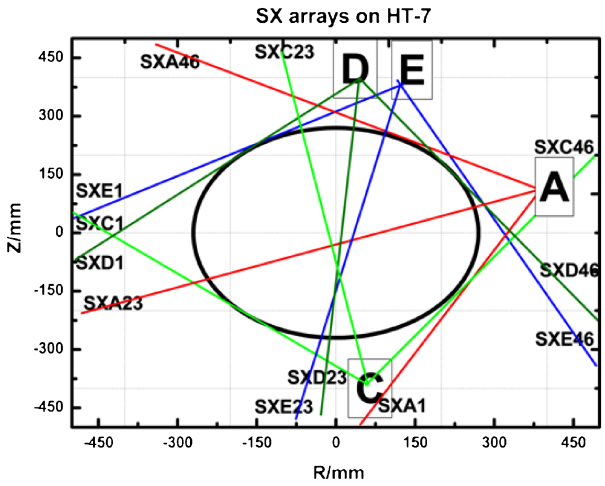

Fig. 1. (Color online) Schematic diagram of the soft x-ray imaging system on HT-7 tokamak. The poloidal view angles of each central chord are: 15° (SXA), 72° (SXE), 84° (SXD), and −80.6° (SXC), where 0° is defined as in the major radius direction. Each array has 46 chords that are numbered clockwise from 1 to 46 (i.e., SXC1 is at the high field side, SXD1 and SXE1 is at the low field side, and SXA1 is at the bottom).

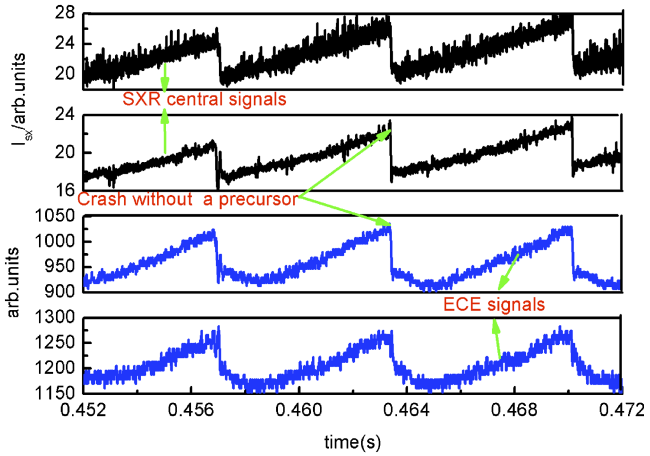

Fig. 2. (Color online) Several crashes in shot #106311 are characterized by the absence of any discernible precursor oscillations. The top 2 rows are SXR central signals, and the bellow 2 rows are ECE (electron temperature) signals.

amplitude (20–30% of the total emission in the central sightline) of the sawtooth crash in LHCD plasmas is helpful for distinguishing the crash and the precursor stage.

There are four available high-resolution soft-x-ray arrays (named SXA, SXC, SXD, and SXE) in one poloidal cross section as shown in Fig. 1. Each array covering the whole plasma region, has 46 channels numbered clockwise from 1 to 46 (i.e., SXC1 is at the high field side, SXD1 and SXE1 are at the low field side and SXA1 is at the bottom). The detector is sensitive to photon energies from 1 to 13 keV. The thickness of the beryllium filter is about 12.5 μm. For each diode, distance from geometric center of plasma to the center of beryllium filter is 400 mm. The maximum sampling rate of this diagnostic system is 250 kHz, corresponding to the temporal resolution 4 μs. Moreover, their spatial resolution is changed from 0.6 to 1.5 cm. The chord integrated soft x-ray signals are transferred to a data storage computer in the control room. Since the contour plot of the reconstructed local emission profile, by using soft-x-ray tomography, mainly reflects the pressure profile, hence the magnetic flux surface, magnetic surface can be obtained by soft-x-ray tomography. The Fourier–Bessel inversion method[31,32] together with the SVD technique[33,34] is used to generate tomographic reconstructions from the high-resolution soft x-ray emission data and this expansion technique is suited to describe the circular plasma across section in the HT-7 tokamak.

3. Observation

We have observed the sawtooth oscillation without any discernible precursor on the intensity signals of the soft x-ray and electron cyclotron emission (ECE) signals in the LHCD discharge (shot #106311) with following plasma parameters: plasma currents $I_p \sim 160$ kA. Central chord-averaged electron density $N_e(0) \sim 3.0 \times 10^{19}$ m^{-3}. Lower Hybrid Wave (LHW) power $P_{lhw} = 320$ kW. Figure 2 shows several crashes in shot #106311 are characterized by the absence of any discernible precursor oscillations. Fast collapse of sawtooth has been observed in both soft x-ray signal and electron cyclotron emission signal in different channels.

The contour plot of the raw data from the soft-x-ray signals of the four arrays of one sawtooth crash in shot #106311 is shown in Fig. 3. The dashed line in each frame corresponds to the crash time at 463.41 ms. It clearly shows that there is almost no clear displacement of the hot core to one direction in all four arrays. In SXA, SXD, and SXE, the profile is flattened simultaneously on both the high field side and the low field side with a little asymmetry. Tomography can give more detailed information about the crash.

Using the SVD analysis, we obtained the spatial structures of soft x-ray emission intensity before and after the crash. Figure 4 shows the results generated with this analysis method. In Fig. 4, the first spatial eigenvector reflects the behavior of equilibrium quantity. The second spatial eigenvector corresponds to the spatial structure of the sawtooth. The higher order components are neglectable here, because the energy they carry is not comparable to the sawtooth. As show in Fig. 4. Since the equilibrium quantity carry almost of the energy of the signal, it is impossible to detect discernible precursor on the intensity signals of the soft x-ray. One can notice that there is no spatial eigenvector corresponds to the spatial structure of the 1/1 mode.

The waveforms of the obtained image are consistent with the waveform of the original. A tomographic reconstruction can be obtained[35] for the change of the plasma is slow enough before and after the crash. The time resolution is 4 μs. The x-ray emission is described by Bessel functions of order m, with lth zero point, $J_m(\lambda_l r)$ which determine the minor-radial dependence and angular harmonics $\sin m\theta$ and $\cos m\theta$. In this paper we take $l = 7$ and $m = 2$.

By using tomography, the reconstructed result of sawtooth oscillation period is shown in Fig. 5. The top row shows the evolution of the line-integrated soft-x-ray signals at three chords. The middle row is the contour plot of the reconstructed local emission intensities profile from the total signals. The bottom row is the contour plot of the reconstructed perturbation of the local emission intensities from the perturbation signals extracted by the SVD method.

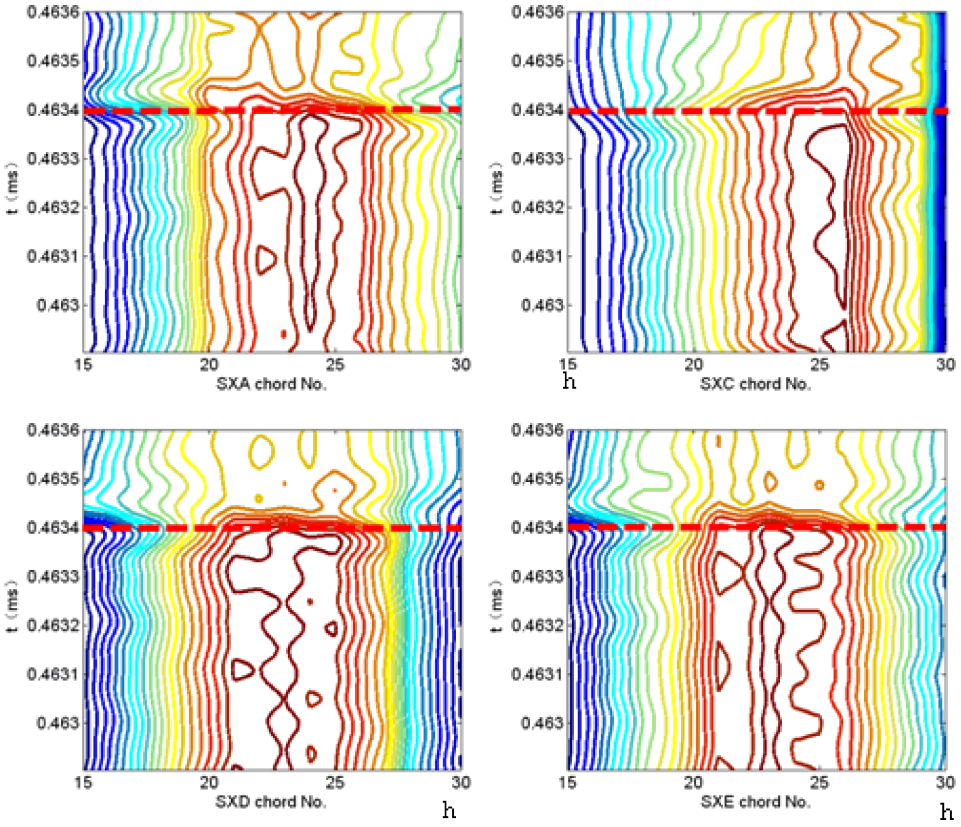

Fig. 3. (Color online) The contour plot of the raw data of the four arrays soft-x-ray signals of a sawtooth crash in shot #106311. The dashed line in each frame corresponds to the crash time at 463.41 ms. The horizontal axis is the channel number (the letter h means the high field side).

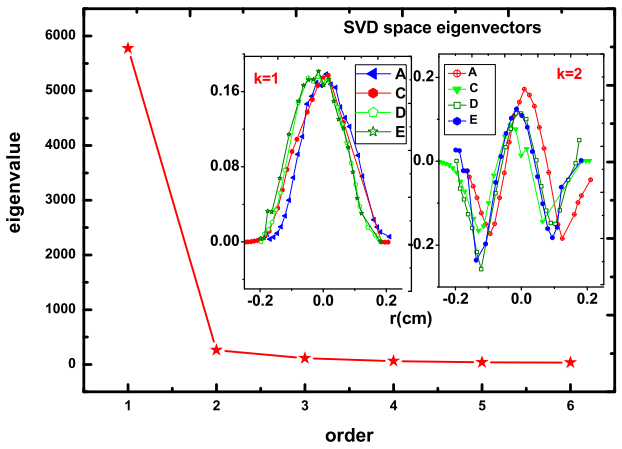

Fig. 4. (Color online) The results of SVD of the shot #106311, the first two components carry all most of the signal energy. The first eigenvector is the equilibrium quantity and the second spatial eigenvector corresponds to the spatial structure of sawtooth.

From the contour plot of the emissivity map, it is very clear that the hot core always stay in the central region of the plasma (A–H in Fig. 5). The hot core outward expansion with symmetry (E in Fig. 5) (the same phenomenon was mentioned in ref. 27). The reconnection progresses occur simultaneously on both the high field side and the low field side with symmetry (D–F in Fig. 5). But different from ref. 27, there is no 1/1 precursor mode in our experimental case. The hot core stay in the central region of the plasma and the profile of emission intensities as shown clearly in Fig. 6.

In order to study reconnection progress and heat transfer progress during sawtooth crash phase, we concentrate on sawtooth collapse phase.

More details about sawtooth collapse phase will be given by tomographic reconstructions as shown in Fig. 7. From the contour plot of the emissivity map, one can clearly see that the profile of emission intensities flatten and hot core outward expansion during sawtooth collapse phase (K–N in Fig. 7). Moreover during the same phase the energy of hot core decrease (J–K in Fig. 7) which means heat outflow (this observation is consistent with ref. 27). The heat outflow (middle of Fig. 8) and the profile of emission intensities flatten (right of Fig. 8) are shown clearly in Fig. 8. It is very clear that large heat outflow during sawtooth crash (the intensity decrease from 117 to 75).

4. Discussion

The above observation strongly suggests that the sawtooth crash is not consistent with the Kadomtsev model. Contour plot of the raw data from the soft-x-ray signals shows that the profile is flattened simultaneously on both the high field side and the low field side with symmetry and tomographic results show that reconnection progresses occur simultaneously on both the high field side and the low field side with symmetry. There is no 1/1 mode during sawtooth period. There must be helical magnetic oscillations exist before sawtooth crash as the result of soft x-ray tomography, but none of discernible precursor oscillation was detected in

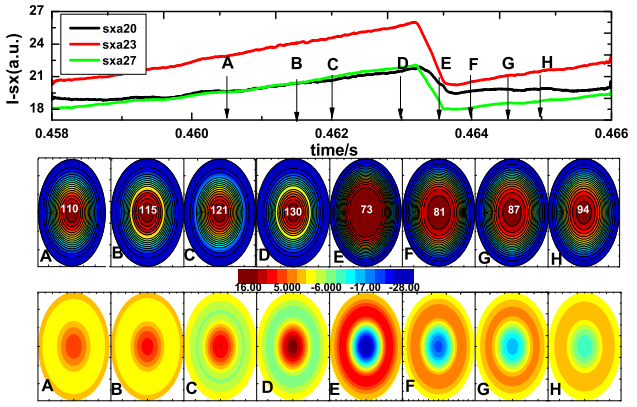

Fig. 5. (Color online) Reconstructed sawtooth period picture by tomography. The top row shows the evolution of the line-integrated soft-x-ray signals at three chords. The middle row is the contour plot of the reconstructed local emission intensities profile from the total signals, and the bottom row is the contour plot of the reconstructed perturbation of the local emission intensities from the perturbation signals extracted by the SVD method. The capital letters on the left of the reconstructed frames correspond to those in the top row frames.

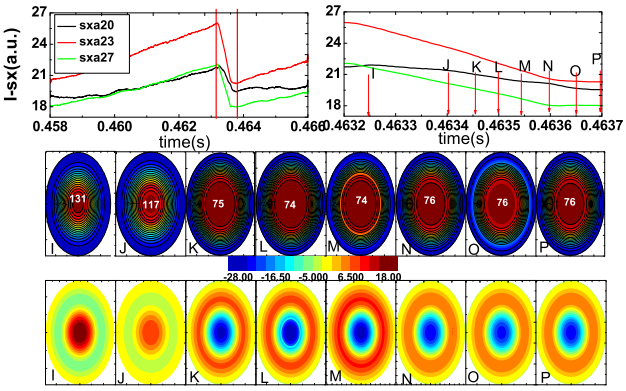

Fig. 7. (Color online) Reconstructed sawtooth crash picture by tomography. The left of top row shows the evolution of the line-integrated soft-x-ray signals at three chords. The right of top row is expanded trace of the specific region in left of top row, and the middle row is the contour plot of the reconstructed local emission intensities profile from the total signals, and the bottom row is the contour plot of the reconstructed perturbation of the local emission intensities from the perturbation signals extracted by the SVD method. The capital letters on the left of the reconstructed frames correspond to those in the top row frames.

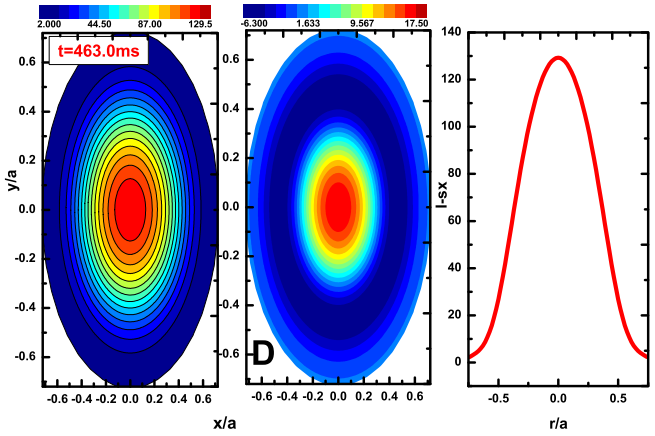

Fig. 6. (Color online) Contour plot of the reconstructed total (left) and perturbation (middle) of local emission intensities of the total signals from the total signals corresponding to the frame (D) in Fig. 5. The right plane is the reconstructed profile of emission intensities.

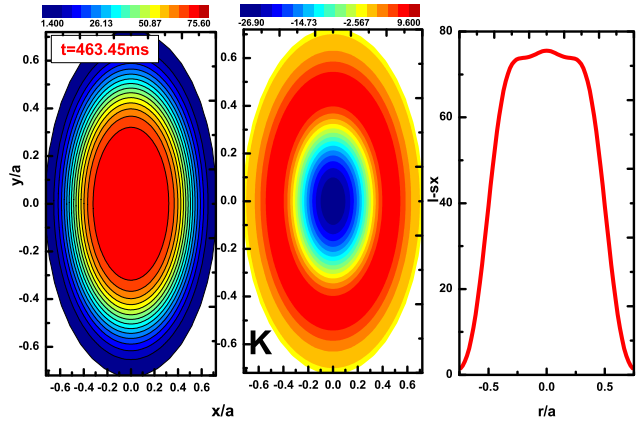

Fig. 8. (Color online) Contour plot of the reconstructed total (left) and perturbation (middle) of the local emission intensities from the total signals corresponding to the frame (K) in Fig. 7. The right plane is the reconstructed profile of emission intensities.

experimental data. The plausible reason for this is that the 1/1 is too small to detect and the growth rate of the 1/1 mode is too fast. The question is why the growth rate of the mode rapidly increased. We suggest that stochastization of magnetic field lines caused rapid sawtooth in HT-7 tokamak.

The time-scale for stochastic temperature diffusion is sufficiently fast to account for the fast sawtooth crash. Resulting of stochastization of magnetic field lines, a transition from semicollisional to collisionless reconnection regimes during non-linear pre-crash phase, hence increased the growth rate of the mode 1/1.

We will consider more details about the reason why temperature is lost during the sawtooth crash. As is known, the hot core includes the largest densities, and its temperature increases more rapidly than other parts. Figure 9 shows the spatial profiles of the soft x-ray emission intensity during one period of the sawtooth oscillation. Variations of the soft x-ray emission intensity roughly reflect the pressure profile. The spatial profiles of soft x-ray emission at time 463.121 ms is more peaked than at time 463.479 ms, and the gradient at the sawtooth reversal surface at time 463.121 ms is larger than at time 463.479 ms. It is suggested that the pressure gradient at the sawtooth reversal surface at time 463.121 ms is larger than that at time 463.479 ms. The peaked soft x-ray profile is broadened after the sawtooth crash at time 463.479 ms. Hence, it is an evidence to prove that temperature is lost during sawtooth crash, which is also consistent with the result of soft x-ray tomography (Fig. 7).

Soft x-ray tomography is an ill-posed problem, and strongly depends on the equilibrium of signals in tokamak case. One should pay attention to the precise of the raw data when using together with Soft x-ray tomography and SVD. Otherwise, the perturbation structure from mathematic calculations will cause an aliasing effect to the real physical structure.

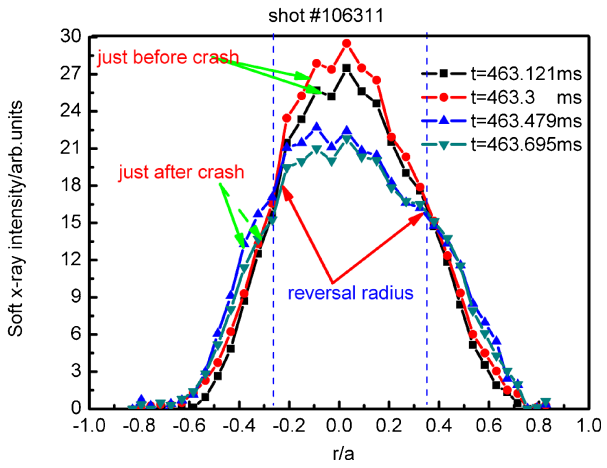

Fig. 9. (Color online) SXR intensity profiles of different time points during a sawtooth crash. The time points 463.121 and 463.3 ms are just before sawtooth crash. The time points 463.479 and 463.695 ms are just after sawtooth crash. Peaked soft x-ray profile is broadened after the sawtooth crash.

5. Conclusion

Two basic phenomena were observed in sawtooth crash in HT-7 tokamak. (1) There is no any discernible precursor oscillation during sawtooth period. (2) Soft-x-ray signals shows that the profile is flattened simultaneously on both the high field side and the low field side with symmetry and a large of the temperature is lost during the sawtooth crash phase. Both the two facts can be explained by stochastization of magnetic field lines in sawtooth oscillations. Although there is no central q value measurement on the HT-7 tokamak, the estimated $q_0 = 0$ is about 0.8–0.85 from the edge q value and sawtooth reversal surface with the assumption of standard monotonic q profile. This just meets the requirement for producing the magnetic stochasticity. So the rapid sawtooth crash in HT-7 may be understood by stochastic model.

Acknowledgements

This work was supported partially by the National Nature Science Foundation of China through grant number 10935004 and was partially supported by the CAS Key International S&T Cooperation Project collaboration with grant number GJHZ1123.

1) S. Von Goeler, W. Stodiek, and N. Sauthoff: Phys. Rev. Lett. **33** (1974) 1201.
2) B. B. Kadomtsev: Sov. J. Plasma Phys. **1** (1975) 389.
3) R. J. Hastie: Astrophysics and Space Science **256** (1998) 177.
4) K. McGuire, V. Arunasalam, C. W. Barnes, M. G. Bell, M. Bitter, R. Boivin, N. L. Bretz, R. Budny, C. E. Bush, A. Cavallo, T. K. Chu, S. A. Cohen, P. Colestock, S. L. Davis, and D. L. Dimock: Phys. Fluids B **2** (1990) 1287.
5) M. A. Dubois, A. L. Pecquet, and C. Reverdin: Nucl. Fusion **23** (1983) 147.
6) F. Porcelli, D. Boucher, and M. N. Rosenbluth: Plasma Phys. Control. Fusion **38** (1996) 2163.
7) A. W. Edwards, D. J. Campbell, W. W. Engelhardt, H.-U. Fahrbach, R. D. Gill, R. S. Granetz, S. Tsuji, B. J. D. Tubbing, A. Weller, J. Wesson, and D. Zasche: Phys. Rev. Lett. **57** (1986) 210.
8) P. Buratti and E. Giovanozzi: 30th EPS Conf. Controlled Fusion and Plasma Physics, 2003, ECA Vol. 27A, 0-1.2A.
9) P. Buratti and E. Giovanozzi: 29th EPS Conf. Controlled Fusion and Plasma Physics, 2002, ECA Vol. 26B, D-5.011.
10) L. Zakhov and B. Rogers: Phys. Fluids B **4** (1992) 3285.
11) F. Porcelli: Phys. Rev. Lett. **66** (1991) 425.
12) J. A. Wesson: Nucl. Fusion **30** (1990) 2545.
13) Y. U. Qingquan: Nucl. Fusion **35** (1995) 1012.
14) X. Wang and A. Bhattacharjee: Phys. Plasmas **2** (1995) 171.
15) A. J. Lichtenberg: Nucl. Fusion **24** (1984) 1277.
16) C. G. Gimblett and R. J. Hastie: Plasma Phys. Control. Fusion **36** (1994) 1439.
17) F. A. Haas and A. Thyagaraja: Plasma Phys. Control. Fusion **37** (1995) 415.
18) V. Igochine, O. Dumbrajs, H. Zohm, and the ASDEX Upgrade Team: Nucl. Fusion **48** (2008) 062001.
19) V. Igochine, O. Dumbrajs, H. Zohm, A. Flaws, and the ASDEX Upgrade Team: Nucl. Fusion **47** (2007) 23.
20) V. Igochine, J. Boom, I. Classen, O. Dumbrajs, S. Günter, K. Lackner, G. Pereverzev, H. Zohm, and ASDEX Upgrade Team: Phys. Plasmas **17** (2010) 122506.
21) V. Igochine, O. Dumbrajs, D. Constantinescu, H. Zohm, G. Zvejnieks, and the ASDEX Upgrade Team: Nucl. Fusion **46** (2006) 741.
22) A. J. Lichtenberg, K. Itoh, S.-I. Itoh, and A. Fukuyama: Nucl. Fusion **32** (1992) 495.
23) K. Chen, L. Hua, Y. Duana, T. Mab, and HT-7 team: Phys. Lett. A **372** (2008) 4469.
24) Ma Tian-Peng, Hu Li-Qun, Wan Bao-Nian, Ruan Huai-Lin, Gao Xiang, Zhen Xiang-Jun, Zhou Li-Wu, Sun You-Wen, Chen Zhong-Yong, Lin Shi-Yao, and Kong Wei: Chin. Phys. **14** (2005) 2061.
25) Y. Sun, B. Wan, L. Hu, S. Wang, B. Shen, X. Zhang, X. Zhen, and G. Xu: Plasma Phys. Control. Fusion **47** (2005) 745.
26) Y. Sun, B. Wan, L. Hu, and B. Shen: Nucl. Fusion **47** (2007) 271.
27) Y. Sun, B. Wan, L. Hu, K. Chen, B. Shen, and J. Mao: Plasma Phys. Control. Fusion **51** (2009) 065001.
28) X. Xu, J. Wang, Y. Wen, Y. Yu, A. Liu, T. Lan, C. Yu, B. Wan, X. Gao, Y. Sun, N. C. Luhmann, Jr., C. W. Domier, Z. G. Xia, and Z. Shen: Plasma Phys. Control. Fusion **52** (2010) 015008.
29) F. X. Soldner, F. Leuterer, R. Bartiromo, S. Bernabei, R. Buchse, O. Gehre, R. W. Harvey, M. Kornherr, K. McCormick, H. D. Murmann, and G. V. Pereverzev: Nucl. Fusion **34** (1994) 985.
30) W. Pfeiffer, F. B. Marcus, C. J. Armentrout, G. L. Jahns, T. W. Petrie, and R. E. Stockdale: Nucl. Fusion **25** (1985) 655.
31) C. Janicki, R. Décoste, and C. Simm: Phys. Rev. Lett. **62** (1989) 3038.
32) Y. Nagayama: J. Appl. Phys. **62** (1987) 2702.
33) C. Nardine: Plasma Phys. Control. Fusion **34** (1992) 1447.
34) M. Anton, H. Weisen, M. J. Dutch, W. von der Linden, F. Buhlmann, R. Chavan, B. Marletaz, P. Marmillod, and P. Paris: Plasma Phys. Control. Fusion **38** (1996) 1849.
35) Y. Nagayama, S. Tsuji, and K. Kawahata: Phys. Rev. Lett. **61** (1988) 1839.